LETTERS

Systematic RNA interference reveals that oncogenic *KRAS*-driven cancers require TBK1

David A. Barbie[1,3,4], Pablo Tamayo[3], Jesse S. Boehm[3], So Young Kim[1,2], Susan E. Moody[1,3], Ian F. Dunn[1,3,5], Anna C. Schinzel[1,3], Peter Sandy[7,8], Etienne Meylan[7,8], Claudia Scholl[6], Stefan Fröhling[6], Edmond M. Chan[3], Martin L. Sos[9], Kathrin Michel[9], Craig Mermel[1,3], Serena J. Silver[3], Barbara A. Weir[3], Jan H. Reiling[7,10], Qing Sheng[1], Piyush B. Gupta[3], Raymond C. Wadlow[3,4], Hanh Le[3], Sebastian Hoersch[8], Ben S. Wittner[3,4], Sridhar Ramaswamy[3,4], David M. Livingston[1], David M. Sabatini[3,7,10,11], Matthew Meyerson[1,2,3], Roman K. Thomas[9,12,13], Eric S. Lander[3,7], Jill P. Mesirov[3], David E. Root[3], D. Gary Gilliland[1,3,6,11], Tyler Jacks[3,7,8,11] & William C. Hahn[1,2,3,6]

The proto-oncogene *KRAS* is mutated in a wide array of human cancers, most of which are aggressive and respond poorly to standard therapies. Although the identification of specific oncogenes has led to the development of clinically effective, molecularly targeted therapies in some cases, *KRAS* has remained refractory to this approach. A complementary strategy for targeting *KRAS* is to identify gene products that, when inhibited, result in cell death only in the presence of an oncogenic allele[1,2]. Here we have used systematic RNA interference to detect synthetic lethal partners of oncogenic *KRAS* and found that the non-canonical IκB kinase *TBK1* was selectively essential in cells that contain mutant *KRAS*. Suppression of *TBK1* induced apoptosis specifically in human cancer cell lines that depend on oncogenic *KRAS* expression. In these cells, TBK1 activated NF-κB anti-apoptotic signals involving c-Rel and BCL-XL (also known as BCL2L1) that were essential for survival, providing mechanistic insights into this synthetic lethal interaction. These observations indicate that TBK1 and NF-κB signalling are essential in *KRAS* mutant tumours, and establish a general approach for the rational identification of co-dependent pathways in cancer.

To identify essential genes in human malignant and non-transformed cell lines, we performed arrayed format RNA interference (RNAi) screens in 19 cell lines (Supplementary Table 1 and Supplementary Fig. 1) using a short hairpin RNA (shRNA) library targeting kinases, phosphatases and oncogenes[3]. We then used two methods to find genes that were selectively required in cells expressing oncogenic *KRAS*. First, we used a class-discrimination feature selection method (Fig. 1a) in which normalized B-scores[4] for each cell line were analysed using a *t*-test statistic[5] to identify the top 250 (5%) shRNAs that distinguished between cell lines that contained mutant or wild-type *KRAS*. We focused on genes in which suppression by at least two shRNAs selectively impaired the proliferation/viability of *KRAS* mutant cells and identified *KRAS* itself (Supplementary Tables 2 and 3 and Supplementary Fig. 2a, b).

In parallel, we used RNAi gene enrichment ranking (RIGER)[6]—a statistical approach that does not rely on arbitrary thresholds—to rank-order candidate *KRAS* synthetic lethal genes (Fig. 1b). RIGER considers all shRNAs for a gene as a 'hairpin set', similar to 'gene sets' in gene set enrichment analysis (GSEA)[7], and provides a normalized enrichment score (NES) for each gene with respect to a specific classification. Using the mutant versus wild-type *KRAS* class distinction as the classification feature, we ranked candidate *KRAS* synthetic lethal partners by NES and selected the top 40 genes, which included 12 of the 17 candidates identified by the individual shRNA-based analysis (Fig. 1b, c and Supplementary Tables 2–4).

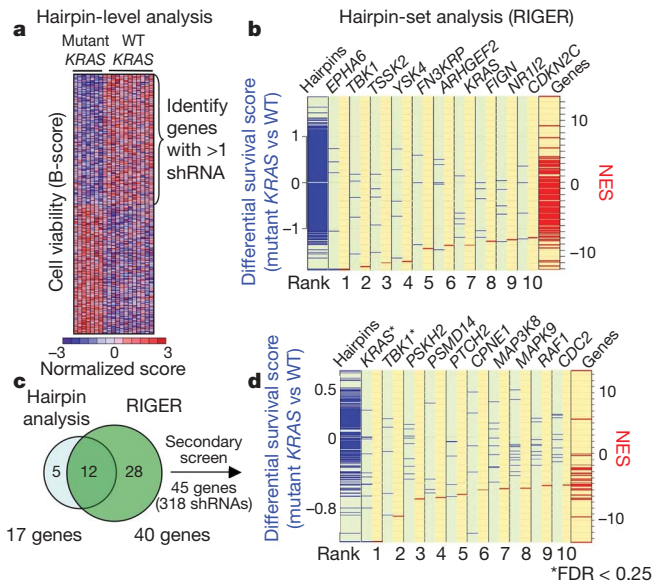

Figure 1 | Meta-analysis of RNAi screens identifying *KRAS* synthetic lethals. a, Supervised analysis of viability data (B-score) identified 250 shRNAs that distinguished mutant *KRAS* from wild-type (WT) cells, including genes targeted by several shRNAs. **b**, Hairpin-set analysis (RIGER). Genes were assigned NESs (red lines) on the basis of *KRAS* mutant/wild-type differential survival scores (blue lines) for each shRNA. Negative values represent mutant *KRAS*-selectivity. **c**, Union of 17 genes identified in **a** and 40 genes identified in **b**. **d**, Secondary screening data normalized using the percentage of control and analysed using RIGER. The FDR values for *KRAS* and *TBK1* were 0.04 and 0.18, respectively.

[1]Department of Medical Oncology, [2]Center for Cancer Genome Discovery, Dana-Farber Cancer Institute, 44 Binney Street, Boston, Massachusetts 02115 USA. [3]Broad Institute of Harvard and M.I.T., 7 Cambridge Center, Cambridge, Massachusetts 02142, USA. [4]Massachusetts General Hospital Cancer Center, 55 Fruit Street, Boston, Massachusetts 02114, USA. [5]Department of Neurosurgery, [6]Department of Medicine, Brigham and Women's Hospital and Harvard Medical School, Boston, Massachusetts 02115, USA. [7]Department of Biology, M.I.T., 77 Massachusetts Avenue, Cambridge, Massachusetts 02139, USA. [8]Koch Institute for Integrative Cancer Research, 40 Ames Street, Cambridge, Massachusetts 02142, USA. [9]Max Planck Institute for Neurological Research with Klaus-Joachim-Zülch Laboratories of the Max Planck Society and the Medical Faculty of the University of Köln, Gleueler Str. 50, 50931 Köln, Germany. [10]Whitehead Institute of Biomedical Research, 9 Cambridge Center, Cambridge, Massachusetts 02142, USA. [11]Howard Hughes Medical Institute, Chevy Chase, Maryland 20815, USA. [12]Department I of Internal Medicine and Center of Integrated Oncology, University of Köln, Gleueler Str. 50, 50931 Köln, Germany. [13]Chemical Genomics Center of the Max-Planck-Society, Otto-Hahn-Str. 15, 44227 Dortmund, Germany.

To validate the 45 candidates identified by these two approaches, we performed a secondary screen on an independent panel of mutant or wild-type *KRAS* lung adenocarcinoma cell lines (Supplementary Figs 3a, b and 4a, b). Proliferation/viability data for each shRNA was normalized to the median value of 20 control shRNAs. Using the *t*-test statistic to rank shRNAs that selectively impaired proliferation/viability in mutant *KRAS* cells, we identified a significantly enriched subset of candidate shRNAs ($P \leq 0.0002$) (Supplementary Fig. 5a). Three *KRAS*-specific shRNAs were among the top four shRNAs that distinguished between *KRAS* mutant and wild-type cell lines (Supplementary Figs 4a, c and 5b). Using RIGER to rank candidate genes with respect to *KRAS*-selective lethality, we identified *KRAS* and *TBK1* as the most significant genes (false discovery rate (FDR) of 0.04 and 0.18, respectively) (Fig. 1d). Although the secondary screen identified other potential *KRAS* synthetic lethal genes, we focused on *TBK1* because it represented the top candidate after *KRAS*.

Indeed, we found that the two top-scoring shRNAs induced *TBK1* suppression and substantial cell death in NCI-H23 cells (mutant *KRAS*) (Fig. 2a). To confirm these findings, we introduced *KRAS*- or *TBK1*-specific shRNAs into a third set of lung cancer cell lines (Fig. 2b), and observed a strong correlation between *KRAS* and *TBK1* dependence, even in cell lines in which *KRAS* mutation status and dependence were decoupled. We also used an isogenic experimental model to isolate the genetic interaction between oncogenic *KRAS* and *TBK1*. Specifically, the expression of oncogenic *KRAS* in immortalized human lung epithelial cells (AALE-K cells)[8] rendered them dependent on both *KRAS* and *TBK1* for survival, as compared to cells expressing a control vector (AALE-V cells) (Fig. 2c). When we suppressed *TBK1* in A549 or NCI-H2009 (mutant *KRAS*) cells, tumour formation was inhibited, whereas the suppression of *TBK1* had no effect on the tumorigenicity of NCI-H1437 or NCI-H1568 (wild-type *KRAS*) cells (Fig. 2d). These observations confirm that cancer cell lines that depend on oncogenic *KRAS* require *TBK1* expression.

To determine whether the suppression of *TBK1* in *KRAS*-dependent cells induced apoptosis, we found that, similar to shRNAs targeting *KRAS* itself (Supplementary Fig. 4b), *TBK1*-specific shRNAs provoked an increase in PARP cleavage (Fig. 2e) and TdT-mediated dUTP nick end labelling (TUNEL)-positive nuclei ($P < 0.01$) (Fig. 2f and Supplementary Fig. 6a) in NCI-H23 cells (mutant *KRAS*) but not in NCI-H1437 cells (wild-type *KRAS*). Suppression of mouse *Tbk1* in cells derived from a *KRAS*-driven murine model of lung cancer (LKR-13 cells)[9] also induced apoptosis (Supplementary Fig. 6b).

KRAS activates several signalling pathways including those regulated by RAF kinases, phosphatidylinositol-3-OH kinases (PI(3)Ks) and RalGEFs (also known as RALGDSs). We found that the suppression of *RAF1*, *BRAF* or *AKT1* failed to kill *KRAS*-dependent lung cancer cell lines selectively (Fig. 2g and Supplementary Fig. 6c). *TBK1* suppression also failed to alter phosphorylated-p42/p44 MAP (mitogen-activated protein) kinase or phosphorylated-AKT levels (Supplementary Fig. 6d). In contrast, the suppression of *RALB* resulted in significant selective lethality in *KRAS*-dependent cell lines ($P < 0.01$, Fig. 2g). Consistent with previous work linking RALB with TBK1 activation in the setting of tumour cell survival[10], this observation suggested that RALB–TBK1 signalling was required in cells that depend on oncogenic *KRAS*.

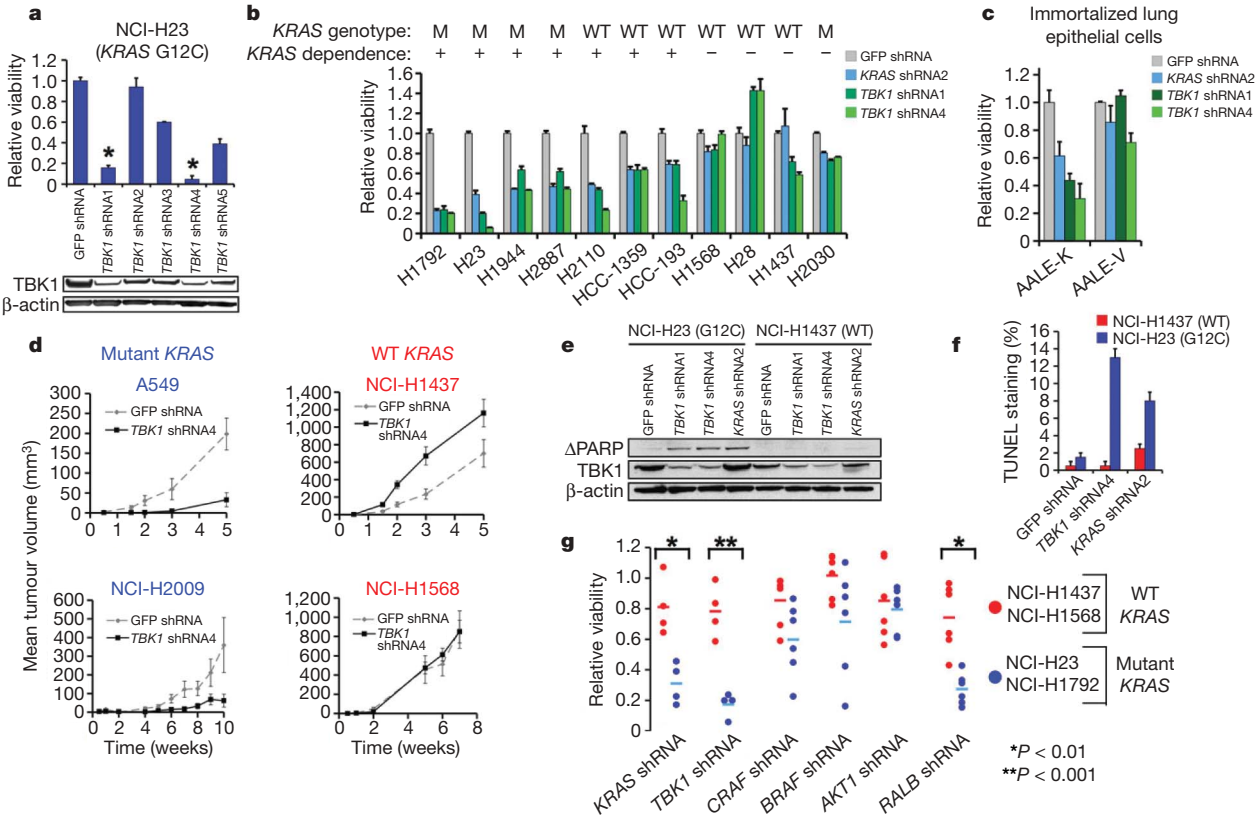

Figure 2 | *TBK1* synthetic lethality with oncogenic *KRAS*. **a**, Top-scoring *TBK1*-specific shRNAs (asterisks) induced lethality and *TBK1* suppression (immunoblot) in NCI-H23 cells (mutant *KRAS*). **b**, Suppression of *KRAS* or *TBK1* in non-small-cell lung cancer (NSCLC) cell lines. HCC-1359 and HCC-193 cells expressed RAS and NF-κB signatures. M, mutant. **c**, *KRAS* and *TBK1* dependence of lung epithelial cells expressing oncogenic *KRAS* (AALE-K) or vector (AALE-V). **d**, Tumour formation after *TBK1* suppression. The mean and s.e.m. of at least 11 replicates are shown. **e**, Immunoblot of cleaved PARP (ΔPARP) after *TBK1* or *KRAS* suppression. **f**, The percentage of TUNEL-positive nuclei after *TBK1* or *KRAS* suppression. Mean and s.d. shown. **g**, Differential cell viability after *KRAS*, *TBK1*, *CRAF*, *BRAF*, *AKT1* or *RALB* suppression using multiple shRNAs in *KRAS* mutant versus wild-type cell lines. $*P < 0.01$, $**P < 0.001$ (*t*-test for comparisons). The s.e.m. of triplicate samples normalized to green fluorescent protein (GFP) shRNA control vector are shown.

TBK1 is a non-canonical IκB kinase that regulates innate immunity through the interferon and NF-κB pathways[11], and is also a component of the exocyst complex[10]. To examine how TBK1 contributes to survival in *KRAS*-dependent cell lines, we performed transcriptional profiling on AALE cells expressing a control vector (AALE-V), oncogenic *KRAS* (AALE-K) or wild-type *KRAS* (AALE-K wild type). Using GSEA to identify gene sets from the Molecular Signatures Database (MSigDB-C2 v2)[7] that were enriched in AALE-K cells, we identified a previously described oncogenic RAS signature[12] as well as several NF-κB pathway activation signatures[13,14] among the most significantly enriched gene sets ($P \leq 4.5 \times 10^{-7}$, hypergeometric test) (Fig. 3a and Supplementary Fig. 7a). In contrast, we failed to detect enrichment of oncogenic RAS or NF-κB signatures in AALE-K wild-type cells (Fig. 3a), indicating that the expression of oncogenic but not wild-type *KRAS* correlated with NF-κB signalling.

To extend these observations to patient-derived tumours, we analysed expression profiles from 128 lung adenocarcinomas[15,16] for expression of the oncogenic RAS[12], NF-κB[13,14] and IRF3 (ref. 17) signatures as well as a *KRAS*-specific signature (AALE-K) composed of the genes most significantly induced in AALE-K relative to AALE-V cells. We found that most mutant *KRAS* tumours (14 out of 19) showed RAS signature activation and co-expression of the NF-κB signature ($P \leq 1.3 \times 10^{-15}$, Spearman correlation test with Bonferroni adjustment) or the IKKε-regulated NF-κB gene subset ($P \leq 0.008$), but not the IRF3-regulated gene set ($P \leq 0.18$) (Fig. 3b). These observations confirm that most lung cancers that contain mutant *KRAS* show evidence of RAS and NF-κB pathway activation, and suggest that a substantial fraction of *KRAS* mutant primary lung cancers may depend on *TBK1* and NF-κB signalling for survival.

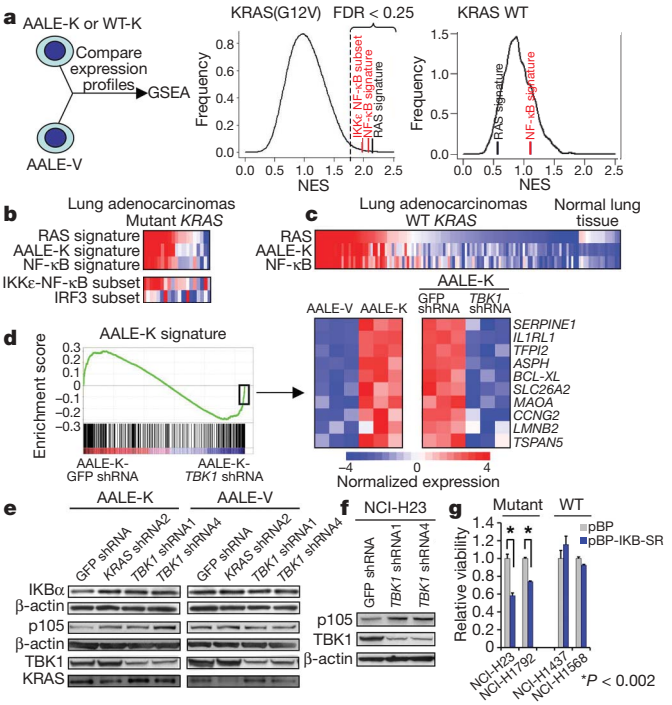

Figure 3 | Oncogenic *KRAS*-induced NF-κB signalling involves TBK1. **a**, GSEA of AALE-V (vector), AALE-K (KRAS(G12V)) or AALE-WT-K (KRAS wild-type) cells (positive NES). A RAS oncogenic signature (black) and NF-κB signatures (red) showed significant enrichment (FDR < 0.25) in AALE-K cells. **b**, RAS signatures in mutant *KRAS* lung adenocarcinomas correlate with NF-κB but not IRF3 signatures (red denotes activation, blue denotes inactivation). **c**, RAS and NF-κB signature expression in wild-type *KRAS* lung adenocarcinomas and normal lung tissue. **d**, AALE-K signature enrichment plot after *TBK1* shRNA or GFP shRNA expression in triplicate samples. Heatmap shows the top *KRAS*-induced genes with negative enrichment in AALE-K-*TBK1* shRNA samples. **e**, **f**, Immunoblot of IKBα, p105, TBK1 and KRAS in AALE-K and AALE-V cells (**e**) or NCI-H23 cells (**f**) after *KRAS* or *TBK1* suppression. **g**, Cell viability after expression of control vector (pBP) or IκBα super-repressor (pBP-IKB-SR) in mutant or wild-type *KRAS* cells. The mean and s.e.m. of triplicate samples are shown, and a *t*-test was used for comparisons. *$P < 0.002$.

Consistent with recent work[18], we also identified RAS and NF-κB signature co-activation in 30 out of 109 *KRAS* wild-type tumours (Fig. 3c). These RAS and NF-κB signatures identified some but not all of the *KRAS* wild-type cell lines that showed *KRAS* dependence (Supplementary Table 1 and Fig. 2b), suggesting that a subset of *KRAS* wild-type tumours depend on TBK1 and NF-κB signalling for survival. Further work will be necessary to determine whether such signatures will prove useful in predicting responsiveness to *TBK1* inhibition.

Although TBK1 activates the interferon pathway through the regulation of IRF3 and IRF7 (refs 10, 11), we failed to observe increased expression of IRF3 target genes[17] (Supplementary Fig. 7b) or increased IRF3 nuclear translocation (Supplementary Fig. 8a) in AALE-K cells. In addition, the suppression of *KRAS* or *TBK1* in *KRAS* mutant cancer cells downregulated specific genes within the NF-κB subset, including *CCND1*, *BCL2* and *IL8*, but failed to alter the expression of known interferon-responsive genes, such as *IFNB1* and *RANTES* (also known as *CCL5*) (Supplementary Fig. 7c). When we suppressed *TBK1* in AALE-K cells, we observed that NF-κB signature components and several NF-κB targets, including the anti-apoptotic gene *BCL-XL*, were among the most significantly downregulated genes (Fig. 3d). These findings confirm the importance of the NF-κB pathway in promoting survival in the setting of oncogenic *RAS*[19], and suggest that, distinct from its role in innate immunity, TBK1 preferentially activates NF-κB signalling in tumours dependent on oncogenic *KRAS*.

TBK1 has been reported to regulate the stability of IκB proteins[11]. When we examined cytoplasmic levels of IκB family members in AALE-K cells, we found reduced levels of IκBα (encoded by *NFKBIA*) and p105 (encoded by *NFKB1*) as compared to AALE-V cells (Fig. 3e and Supplementary Fig. 8a, b). Moreover, the suppression of *TBK1* in AALE-K cells or *KRAS*-mutant NCI-H23 cells (Fig. 3e, f) returned levels to that observed in wild-type *KRAS* cells. The expression of the IκBα super-repressor (IKB-SR)[20], which inhibits NF-κB activity, in AALE-K, AALE-V or cancer cell lines expressing mutant or wild-type *KRAS* induced cell death specifically in cells containing mutant *KRAS* (Fig. 3g and Supplementary Fig. 9). These findings confirm that TBK1-driven NF-κB activity promotes the survival of cells that depend on mutant *KRAS*.

In the primary shRNA screen, we noted that one shRNA targeting the NF-κB family member *c-Rel* (also known as *REL*) scored as selectively lethal in *KRAS* mutant cells, albeit just below our pre-determined threshold. Suppression of *c-Rel* but not *IRF3* selectively induced apoptosis in *KRAS* mutant cells ($P \leq 0.001$) (Fig. 4a and Supplementary Fig. 10a). Moreover, we found that the suppression of *TBK1* in *KRAS* mutant cancer cells reduced the total and nuclear c-Rel levels (Fig. 4b and Supplementary Fig. 10b). Although TBK1 can phosphorylate c-Rel when overexpressed[21], we failed to detect an interaction between TBK1 and c-Rel, but confirmed that endogenous c-Rel and p105 interact (Supplementary Fig. 10c)[22].

Because *BCL-XL*, a known c-Rel target[23], was identified as a TBK1-regulated gene in AALE-K cells (Fig. 3d), we examined the expression of several anti-apoptotic genes after *TBK1* suppression in *KRAS*-mutant cancer cells, and observed specific downregulation of *BCL-XL* in several cell lines (Fig. 4b and Supplementary Fig. 10d). Moreover, the overexpression of BCL-XL rescued apoptosis induced by *KRAS* or *TBK1* suppression in NCI-H23 cells (Fig. 4c, d) but did not significantly affect cell death induced by the suppression of *BIRC5* (also known as survivin) (Supplementary Fig. 11), confirming p105, c-Rel and BCL-XL as mediators of NF-κB survival signalling downstream of TBK1 and KRAS.

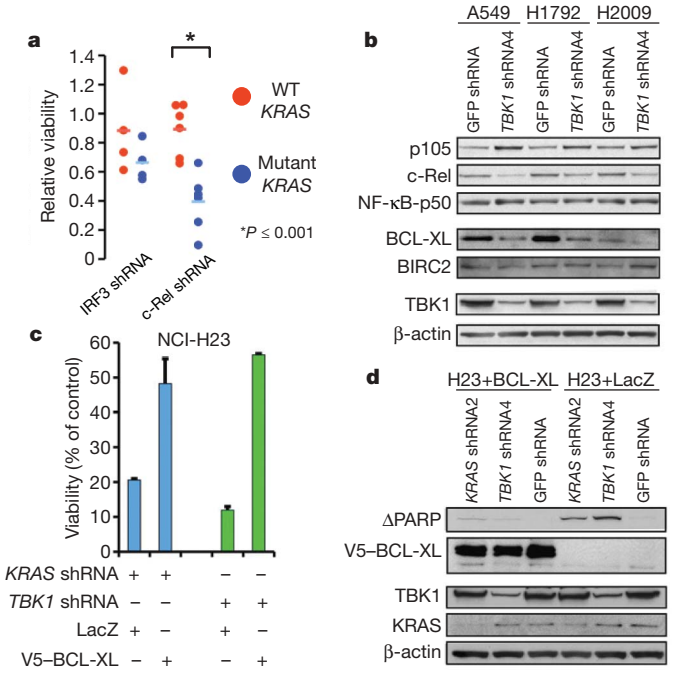

Figure 4 | TBK1 regulates c-Rel and BCL-XL in *KRAS* mutant cells. **a**, Differential cell viability after *IRF3* or *c-Rel* suppression using multiple shRNAs in *KRAS* mutant versus wild-type cell lines. **b**, Immunoblot of p105, NF-κB-p50 (cleavage product of p105), c-Rel, BCL-XL and BIRC2 in *KRAS* mutant cell lines after *TBK1* suppression. **c**, Cell viability after *KRAS* or *TBK1* suppression in NCI-H23 cells expressing a control protein (LacZ) or V5-tagged BCL-XL. The s.e.m. of triplicate samples normalized to GFP shRNA control vector are shown. **d**, Immunoblot showing overexpression of V5-tagged BCL-XL and inhibition of PARP cleavage.

We have identified *TBK1* as a synthetic lethal partner of oncogenic *KRAS*. These findings link RALB-mediated activation of TBK1 (ref. 10) to the generation of specific NF-κB-regulated survival signals downstream of oncogenic *KRAS*. Furthermore, although studies testing the effects of inhibiting TBK1 or NF-κB signalling in established tumours are necessary, *TBK1* and more generally NF-κB signalling may represent an alternative method of targeting oncogenic *KRAS*-driven cancers. Recently, *STK33* and *PLK1* were identified as *KRAS* synthetic lethal partners by the application of RNAi screening in paired *KRAS* mutant and wild-type cell lines[24,25]. Both genes were also identified in our computational analyses (Supplementary Tables 3 and 4), but like *c-Rel*, they fell below our initial threshold for secondary screening. We anticipate that the development of fully validated shRNA libraries, coupled with the interrogation of larger numbers of cell lines, will permit saturating genetic screens to identify synthetic lethal partners of *KRAS* as well as other oncogenes and tumour suppressor genes. More generally, this and other studies[6,24–28] indicate that the application of these functional and analytical approaches will facilitate the comprehensive identification of functional co-dependencies in cancer.

METHODS SUMMARY

Large-scale, arrayed format RNAi screens to identify genes essential for proliferation/viability were performed as described[3,14]. The effect of introducing each of the 5,002 shRNAs (targeting 957 genes) was determined in 19 cell lines, and normalized using the B-score metric[4]. Feature selection of shRNA B-score data was performed using the Comparative Marker Application Suite in GenePattern[5] and was independently analysed using RIGER analysis[6] to compute NESs for each gene. Secondary screen viability data was normalized using a percentage of the control statistic, given the biased nature of the candidate shRNA plate. Expression profiling was used to generate a signature that correlates with *KRAS* activation and implicated NF-κB signalling in cell lines and tumours dependent on *KRAS*. Regulation of NF-κB by TBK1 was shown using biochemical and cell biological approaches. Details of the analytical methods are provided in the Methods.

Full Methods and any associated references are available in the online version of the paper at www.nature.com/nature.

Received 23 January; accepted 27 August 2009.
Published online 21 October 2009.

1. Hartwell, L. H., Szankasi, P., Roberts, C. J., Murray, A. W. & Friend, S. H. Integrating genetic approaches into the discovery of anticancer drugs. *Science* **278,** 1064–1068 (1997).
2. Kaelin, W. G. Jr. The concept of synthetic lethality in the context of anticancer therapy. *Nature Rev. Cancer* **5,** 689–698 (2005).
3. Moffat, J. *et al.* A lentiviral RNAi library for human and mouse genes applied to an arrayed viral high-content screen. *Cell* **124,** 1283–1298 (2006).
4. Malo, N., Hanley, J. A., Cerquozzi, S., Pelletier, J. & Nadon, R. Statistical practice in high-throughput screening data analysis. *Nature Biotechnol.* **24,** 167–175 (2006).
5. Gould, J., Getz, G., Monti, S., Reich, M. & Mesirov, J. P. Comparative gene marker selection suite. *Bioinformatics* **22,** 1924–1925 (2006).
6. Luo, B. *et al.* Highly parallel identification of essential genes in cancer cells. *Proc. Natl Acad. Sci. USA* **105,** 20380–20385 (2008).
7. Subramanian, A. *et al.* Gene set enrichment analysis: a knowledge-based approach for interpreting genome-wide expression profiles. *Proc. Natl Acad. Sci. USA* **102,** 15545–15550 (2005).
8. Lundberg, A. S. *et al.* Immortalization and transformation of primary human airway epithelial cells by gene transfer. *Oncogene* **21,** 4577–4586 (2002).
9. Wislez, M. *et al.* Inhibition of mammalian target of rapamycin reverses alveolar epithelial neoplasia induced by oncogenic K-ras. *Cancer Res.* **65,** 3226–3235 (2005).
10. Chien, Y. *et al.* RalB GTPase-mediated activation of the IκB family kinase TBK1 couples innate immune signaling to tumor cell survival. *Cell* **127,** 157–170 (2006).
11. Häcker, H. & Karin, M. Regulation and function of IKK and IKK-related kinases. *Sci. STKE* **2006,** re13 (2006).
12. Bild, A. H. *et al.* Oncogenic pathway signatures in human cancers as a guide to targeted therapies. *Nature* **439,** 353–357 (2006).
13. Hinata, K., Gervin, A. M., Jennifer Zhang, Y. & Khavari, P. A. Divergent gene regulation and growth effects by NF-κB in epithelial and mesenchymal cells of human skin. *Oncogene* **22,** 1955–1964 (2003).
14. Boehm, J. S. *et al.* Integrative genomic approaches identify *IKBKE* as a breast cancer oncogene. *Cell* **129,** 1065–1079 (2007).
15. Ding, L. *et al.* Somatic mutations affect key pathways in lung adenocarcinoma. *Nature* **455,** 1069–1075 (2008).
16. Takeuchi, T. *et al.* Expression profile-defined classification of lung adenocarcinoma shows close relationship with underlying major genetic changes and clinicopathologic behaviors. *J. Clin. Oncol.* **24,** 1679–1688 (2006).
17. Andersen, J., VanScoy, S., Cheng, T. F., Gomez, D. & Reich, N. C. IRF-3-dependent and augmented target genes during viral infection. *Genes Immun.* **9,** 168–175 (2008).
18. Singh, A. *et al.* A gene expression signature associated with "K-Ras addiction" reveals regulators of EMT and tumor cell survival. *Cancer Cell* **15,** 489–500 (2009).
19. Mayo, M. W. *et al.* Requirement of NF-κB activation to suppress p53-independent apoptosis induced by oncogenic Ras. *Science* **278,** 1812–1815 (1997).
20. Brown, K., Gerstberger, S., Carlson, L., Franzoso, G. & Siebenlist, U. Control of IκB-α proteolysis by site-specific, signal-induced phosphorylation. *Science* **267,** 1485–1488 (1995).
21. Harris, J. *et al.* Nuclear accumulation of cRel following C-terminal phosphorylation by TBK1/IKKε. *J. Immunol.* **177,** 2527–2535 (2006).
22. Mercurio, F., DiDonato, J. A., Rosette, C. & Karin, M. p105 and p98 precursor proteins play an active role in NF-κB-mediated signal transduction. *Genes Dev.* **7,** 705–718 (1993).
23. Owyang, A. M. *et al.* c-Rel is required for the protection of B cells from antigen receptor-mediated, but not Fas-mediated, apoptosis. *J. Immunol.* **167,** 4948–4956 (2001).
24. Scholl, C. *et al.* Synthetic lethal interaction between oncogenic KRAS dependency and STK33 suppression in human cancer cells. *Cell* **137,** 821–834 (2009).
25. Luo, J. *et al.* A genome-wide RNAi screen identifies multiple synthetic lethal interactions with the Ras oncogene. *Cell* **137,** 835–848 (2009).
26. Ngo, V. N. *et al.* A loss-of-function RNA interference screen for molecular targets in cancer. *Nature* **441,** 106–110 (2006).
27. Rottmann, S., Wang, Y., Nasoff, M., Deveraux, Q. L. & Quon, K. C. A. TRAIL receptor-dependent synthetic lethal relationship between MYC activation and GSK3β/FBW7 loss of function. *Proc. Natl Acad. Sci. USA* **102,** 15195–15200 (2005).
28. Silva, J. M. *et al.* Profiling essential genes in human mammary cells by multiplex RNAi screening. *Science* **319,** 617–620 (2008).

Supplementary Information is linked to the online version of the paper at www.nature.com/nature.

Acknowledgements This work was supported in part by grants from the US National Cancer Institute (R33 CA128625, R01 CA130988) (W.C.H.) and NIH T32 CA09172-33 (D.A.B., S.E.M.), the Starr Cancer Consortium (I1-A11; W.C.H., D.G.G.), the Susan Madden Fund and an ASCO YIA (D.A.B.), a Department of Defense Prostate Cancer Postdoctoral Fellowship (S.Y.K.), a Brain Science Foundation Fellowship (I.F.D.), the Deutsche Krebshilfe (grant 107954) (R.K.T.),

the Fritz-Thyssen-Stiftung (grant 10.08.2.175; R.K.T.) and the NGFNplus-program of the German Ministry of Science and Education (BMBF, grant 01GS08100; R.K.T.). We thank C. Yu, G. Wei and members of the Hahn laboratory for discussions. High-throughput RNAi screening was conducted at the RNAi Platform of the Broad Institute of MIT and Harvard.

Author Contributions D.A.B., J.S.B., S.Y.K., S.E.M. and W.C.H. designed the experiments. D.A.B. and P.T. performed computational analyses. S.Y.K., I.F.D., A.C.S., P.S., C.S., S.F., P.B.G., J.H.R., Q.S. and R.C.W. performed primary RNAi screens; S.J.S., S.H., B.S.W., C.M. and B.A.W. assisted with data analysis. D.A.B. performed secondary screen with help from H.L. S.E.M. performed tumour xenograft experiments. E.M. performed experiments with murine cell lines. D.A.B., J.S.B., E.M.C., M.L.S., K.M. and R.K.T. performed expression-profiling experiments. S.R., D.M.L., D.M.S., E.S.L., D.G.G., T.J. and D.E.R. supervised RNAi screens; M.M. and J.P.M. supervised data analysis. D.A.B. and W.C.H. wrote the manuscript. W.C.H. coordinated all aspects of the project. All authors discussed results and edited the manuscript.

Author Information All microarray data are available from the Gene Expression Omnibus database (http://www.ncbi.nlm.nih.gov/geo) under accession codes GSE17671, GSE17672 and GSE17643. Reprints and permissions information is available at www.nature.com/reprints. The authors declare competing financial interests: details accompany the full-text HTML version of the paper at www.nature.com/nature. Correspondence and requests for materials should be addressed to W.C.H. (william_hahn@dfci.harvard.edu).

METHODS

RNAi screens. Large-scale RNAi arrayed format screening was conducted using a subset of the Broad Institute RNAi Consortium (TRC) shRNA library targeting kinases, phosphatases and other cancer-related genes[3,14]. shRNA designs and protocols for high throughout lentiviral production are available at http://www.broad.mit.edu/rnai/trc/lib. Cells were seeded in quadruplicate 384-well plates on day 0, followed by infection with 8 μg ml^{-1} polybrene on day 1. Puromycin selection for duplicate plates (concentration individualized per cell line, most cell lines 2 μg ml^{-1}) was started on day 2. An ATP-based luminescence assay (Cell-Titer Glo, Promega) was used to determine the cell number on day 6. Raw luminescence values from duplicate plates were averaged, and the ratio of puromycin-positive to -negative values was used to assess infection efficiency. Data was normalized using the B-score metric—a variant of the *Z*-score that uses the median absolute deviation to account for plate-to-plate variability—as well as a two-way median polish to minimize row/column effects[4]. After excluding shRNAs with low infection efficiency, B-score values from puromycin-positive and -negative replicates were averaged for each shRNA. shRNA B-score values were aligned for the 5,002 shRNAs tested in all 19 cell lines. The secondary screen was conducted using a percentage of control statistic instead of the B-score.

Hairpin-level analysis. The meta-analysis of RNAi screens was performed using complementary computational approaches. The first involved conversion of the shRNA B-score file into a .res file format for input into the Comparative Marker Selection application suite in GenePattern, along with a standard classification file to generate class distinctions[5]. This method uses class discrimination feature selection and ranks shRNA B-score data by the *t*-test statistic or the signal-to-noise ratio to account for the difference in means between the two classes as well as the standard deviation across samples. Specifically, the difference in mean viability scores induced by each shRNA in the *KRAS* mutant class versus the wild-type class was normalized to its standard deviation using a *t*-test, and shRNAs were ranked by the *t*-test score to determine for class selective effects. To convert shRNA data to candidate genes and to reduce the likelihood of off-target effects, the top 250 (5%) of distinguishing shRNAs in the mutant *KRAS* class were filtered to identify several shRNAs targeting the same gene. Only those genes for which at least one shRNA yielded a mean B score <-1 across the KRAS mutant class were considered. Furthermore, shRNAs with low infection efficiency in several cell lines were excluded from the analysis.

RIGER analysis. Similar to gene sets for GSEA[7], hairpin sets were defined as the groups of shRNAs representing a given target gene. Because the number of shRNAs in a hairpin set are relatively small compared with the number of genes, we used different input data normalization, enrichment statistics and output formats compared with GSEA. RIGER analysis consisted of the following steps:

(1) Pre-processing: the input was the same data set of B-scores analysed using the individual shRNA-based method. The B-score values for each cell line were standardized with respect to the median and maximum absolute deviation of the set of control shRNAs (directed against GFP, LacZ, RFP and luciferase) in the same cell line. This centred and rescaled the values in a sample-specific manner according to the behaviour of the control hairpins. After normalization, values below -3 and above 3 were truncated to -3 and 3, respectively, to reduce the effect of outliers, and were called normalized survival scores.

(2) Feature ranking: after pre-processing, each shRNA was assigned a 'differential survival score', which represented the difference in means of the normalized survival scores in the two phenotypic classes (for example, *KRAS* mutant versus wild type). The difference in means was used to emphasize the absolute magnitude of the survival differences and not only the profile 'shape'. Specifically, this favoured shRNAs with strong differential killing of cells over ones that exhibited weak differential killing of cells, but had perfect discrimination profiles inside classes. The differential survival scores were computed for all the 5,002 shRNAs and sorted from high to low scores.

(3) Calculation of enrichment scores: a given gene was assigned an enrichment score according to the distribution of differential survival scores of its shRNAs within the rank list of all shRNAs using a two-sample weighted 'Zhang C' statistic based on the likelihood ratio[29]. The Zhang C likelihood ratio statistic was used owing to its greater sensitivity and better empirical results in exploratory analyses with other data sets. We adapted this method to separate positive and negative enrichment contributions, and used a weighting factor based on the differential enrichment score, except for scores between -0.5 and 0.5, which were truncated to reduce the effects of shRNAs that weakly distinguished classes. The enrichment score obtained in this manner was representative of both the extremeness of the shRNA differential survival scores for a given gene and their consistency.

(4) Normalization of enrichment scores: because genes with different numbers of shRNAs were assigned enrichment scores on different scales, we normalized them before sorting the genes by using a null distribution generated by 1,000 random permutations of the locations of the shRNAs in the entire list. The normalization for negative enrichment scores was a rescaling by the absolute value of the mean of the negative values in the null distribution. This represented an effective way to place the enrichment scores on a common scale regardless of the number of shRNAs for each gene. The null distribution also provided nominal *P* values for each gene enrichment score.

(5) Generation of results: the analysis resulted in a list of genes sorted by their NESs, and a set of complementary estimates of statistical significance, such as nominal, family-wise and Bonferroni *P* values plus a FDR. A collection of dual-vertical plots was used to demonstrate the shRNA differential survival scores for each gene (lines in blue) and NESs (lines in red). Vertical plots were arranged starting with the top gene (strongest negative NES) on the left.

Secondary screen. Analysis of secondary screen data followed the same methodology except for the normalization of the cell proliferation/viability data. Twenty control shRNAs directed against RFP, LacZ and luciferase were screened in parallel with candidates. We normalized data for each shRNA in each cell line using the percentage of control statistic, dividing the raw data for each shRNA by the median of control shRNA values, and taking the $\log_{10}$ of this number to scale values around zero. Because of the biased nature of the candidate shRNA plate, and because the number of control shRNAs was smaller in the secondary screen than the first, the calculation of the maximum absolute deviation was noisy and unreliable. No truncation was applied to the resulting values.

A larger set of 84 control shRNAs directed against GFP, RFP, LacZ and luciferase was also tested independently in all eight cell lines chosen for the secondary screen. We normalized data for each shRNA in each cell line by dividing the raw data for each control shRNA by the plate median and taking the $\log_{10}$ of this number to scale values around zero. We used the *t*-test statistic to examine the *KRAS* mutant versus wild-type class distinction for this control plate relative to the candidate plate, restricting the analysis to shRNAs with strong effects on proliferation/viability (mutant *KRAS* class mean log percentage of control <-0.2, corresponding to $\sim$37% viability impairment) (Supplementary Fig. 5a). We used the *t*-test statistic threshold that was achieved by the set of control shRNAs as the boundary to identify the top 25 shRNAs *KRAS* synthetic lethal shRNAs that scored on the candidate plate (Supplementary Fig. 5b)

Gene expression profiling or GSEA. RNA was prepared from AALE cells expressing KRAS(G12V) or a control vector 6 days after infection and analysed using human U133A HTA Arrays (Affymetrix). GSEA was performed using gene sets from the Molecular Signatures Database (MSigDB-C2 v2)[7]. In brief, the method consists of the following steps: genes are first ranked in a list, L, by the correlation between their expression and the class distinction (for example, *KRAS* mutant versus wild type), using a suitable correlation metric. Given a defined set of genes S (for example, genes members of a signalling pathway, located in the same genomic region, sharing the same Gene Ontology category, and so on), the goal of GSEA is to determine whether the members of S are found at the top or bottom of the list, indicating that they associate with the phenotypic distinction, rather than being distributed uniformly or randomly across the list. Next, to evaluate this degree of 'enrichment', an enrichment score is calculated to quantify the degree to which a set S is over-represented at the top or bottom of the entire ranked list L. After calculation of the scores for a collection of gene sets, an empirical phenotype-based permutation test procedure is used to estimate *P* values. The permutation of class labels preserves gene–gene correlations and provides an assessment of significance that is more reflective of the underlying biology. Finally, an adjustment is made to the estimated significance level to account for multiple hypotheses testing. GSEA normalizes the enrichment score for each gene set to account for the variation in set sizes, yielding a NES and a FDR. The FDR gives an estimate of the probability that a set with a given NES represents a false-positive finding; it is computed by comparing the tails of the observed and permutation-computed null distributions for the NES. The collection of gene sets used in the analysis of Fig. 3a consisted of release 2.5 of the C2 (curated gene sets) sub-collection of the Molecular Signatures Database (http://www.broad.mit.edu/gsea/msigdb/). To determine the significance of identifying many NF-κB upregulated gene sets enriched in AALE-K cells, we used a hypergeometric test.

Gene expression profiling was also performed in triplicate in AALE-K cells (KRAS(G13D)) 5 passages after stable integration of the *KRAS* allele and compared with AALE-V cells using human U133A Arrays (Affymetrix). We created a new *KRAS*-specific gene signature using the mean difference in expression between AALE-K and AALE-V triplicate samples to determine the 300 most significantly induced genes by oncogenic *KRAS*. In parallel, expression profiling was performed in AALE-K cells 48 h after expression of GFP shRNA or *TBK1* shRNA, to identify which of these genes were most significantly downregulated after *TBK1* suppression.

Signature projection method. The RAS oncogenic signature[12], AALE-K signature, NF-κB signature[13], IKKε-regulated NF-κB gene set[14] and IRF3 target gene set[17] were projected across 38 lung adenocarcinomas derived from the

Tumour Sequencing Project[15], an additional 90 lung adenocarcinomas[16], a collection of 53 lung cancer cell lines[30], and 17 normal lung tissue specimens[31]. This was accomplished by a 'single sample' extension of GSEA[7] that allows one to define an enrichment score that represents the degree of absolute enrichment of a gene set in each sample within a given data set. The gene expression values for a given sample were rank-normalized, and an enrichment score was produced using the Empirical Cumulative Distribution Functions (ECDF) of the genes in the signature and the remaining genes. This procedure is similar to GSEA but the list is ranked by absolute expression (in one sample). The enrichment score is obtained by an integration of the difference between the ECDF. For a given signature G of size N_G and single sample S, of the data set of N genes, the genes are replaced by their ranks according the their absolute expression from high to low: $L=\{r_1,r_2,...,r_N\}$. An enrichment score $ES(G,S)$ is obtained by a sum (integration) of the difference between a weighted ECDF of the genes in the signature P_G^w and the ECDF of the remaining genes P_{N_G}:

$$ES(G,S)=\sum_{i=1}^{N}[P_G^w(G,S,i)-P_{N_G}(G,S,i)]$$

$$\text{where } P_G^w(G,S,i)=\sum_{r_j\in G,j\le i}\frac{|r_j|^\alpha}{\sum_{r_j\in G}|r_j|^\alpha}$$

$$\text{and } P_{N_G}(G,S,i)=\sum_{r_j\notin G,j\le i}\frac{1}{(N-N_G)}$$

This calculation is repeated for each signature and each sample in the data set. Note that the exponent of this quantity (α) is set to 1/4, and adds a modest weight to the rank. In the regular GSEA a similar enrichment score is used, but the weight is typically set to 1. Also, instead of the sum over i, the enrichment score is computed according to the largest difference. This quantity is slightly more robust and more sensitive to differences in the tails of the distributions than the Kolmogorov–Smirnov statistic. It is particularly well suited to represent the activation score of gene sets on the basis of a relatively small subset of the genes attaining high expression values. Signature values were normalized using the entire set of 128 lung adenocarcinomas and 17 normal lung specimens. P values were calculated for the lung adenocarcinoma samples testing the hypotheses that the Spearman correlation between the RAS oncogenic signature, NF-κB gene set, and IRF3 target gene set were greater than zero.

Cell culture. 293T and A549 cells were grown in DMEM supplemented with 10% FBS, 2 mM L-glutamine, penicillin (1,000 U ml^{-1}) and streptomycin (1,000 μg ml^{-1}). NCI-H23, NCI-H28, HCC-193, NCI-H522, HCC-1359, NCI-H1437, NCI-H1568, NCI-H1792, NCI-H1944, NCI-H1975, NCI-2009, NCI-H2030, NCI-H2110 and NCI-H2887 cells were cultured in RPMI supplemented with 10% FBS, 2 mM L-glutamine, penicillin and streptomycin. AALE cells[8] were cultured in serum-free SABM media with SingleQuot supplements/growth factors (Lonza). AALE cells expressing KRAS(G12V) or KRAS(G13D) alleles were generated after transduction using a pBabe retroviral vector or pLenti6.2/V5-Dest lentiviral vector (Invitrogen) respectively, as described[14]. Cell lines expressing the IKBα super-repressor were generated using a pBabe retroviral vector expressing the IKBα super-repressor[14], and NCI-H23 cells expressing BCL-XL or LacZ were generated using pLenti6.2/V5-Dest encoding either BCL-XL or LacZ. Cells were seeded in 96-well plates for cell viability assays, and in 6-well plates to prepare lysates for immunoblotting.

Low throughput lentiviral shRNA production/infection. Lentiviral vectors encoding shRNAs specific for control GFP sequences as well as *KRAS*, *TBK1*, *CRAF*, *BRAF*, *AKT1*, *RALB*, *IRF3*, *c-Rel* and *BIRC5* are part of the TRC shRNA library. Sequences of validated shRNAs are listed in Supplementary Table 6. Lentiviruses were produced by transfection of 293T cells with vectors encoding gene-specific shRNAs (1 μg) together with the packaging plasmids encoding Δ8.9 and VSV-G using Fugene 6 (Roche). Culture supernatants containing lentivirus were collected 48 and 72 h after transfection. Virus was pooled and stored at −80 °C. Cells were infected using a 1:11 dilution of virus in polybrene-containing media. After centrifugation at 1,000*g* for 15 min, all NSCLC lines were selected in puromycin (2 μg ml^{-1}) starting 24 h after infection. AALE cells were treated with virus/polybrene for 4 h and selected with puromycin (1 μg ml^{-1}). Viability assays were conducted 6 days after infection using Cell-Titer Glo (Promega) in triplicate. Lysates were collected 72 h after shRNA expression to assess gene suppression. To determine differential viability effects in NCI-H23/NCI-H1792 (mutant *KRAS*) versus NCI-H1437/NCI-H1568 (wild-type *KRAS*) cells, mean viability for each shRNA was normalized to GFP shRNA control. Results from validated shRNAs were grouped together for each gene in KRAS mutant versus wild-type cell lines, and an unpaired *t*-test was used to determine statistical significance.

Antibodies. Immunoblotting was performed as described[14]. Antibodies were obtained from Cell Signaling Technology (anti-AKT1 no.2967, anti-phosho-AKT Ser 473 no.9271, anti-BCL-XL no.2762, anti-BIRC2 no.4952, anti-CRAF no.9422, anti-c-Rel no.4727, anti-GAPDH no.2118, anti-IKBα no.4814, anti-Lamin A/C no.2032, anti-phospho-MAPK p42/44 no.9102, anti-p105/p50 no.3035, anti-PARP cleaved Asp 214 no.9546, anti-RALB no.3523 and anti-survivin no.2808), Santa Cruz Technology (anti-KRAS sc-30, anti-B-RAF F-7, anti-IRF3 FL-425 and anti-IKBα c-15), and Upstate Biotechnologies/Millipore (anti-TBK1 clone AOW9).

Tumorigenicity assay. Tumour xenograft experiments were performed as described[14]. Control GFP or *TBK1*-specific shRNAs were expressed in the indicated cells for 72 h, and 2×10^6 viable cells were then injected subcutaneously per site into immunodeficient mice. The mean and s.e.m. tumour volume were plotted over time. The total number of tumours/implantations were: A549-GFP shRNA (10/13); A549-*TBK1* shRNA (0/11); NCI-H1437-GFP shRNA (12/12); NCI-H1437-*TBK1* shRNA (12/12), NCI-1568-GFP shRNA (12/12); NCI-1568-*TBK1* shRNA (12/12); NCI-H2009-GFP shRNA (9/12); NCI-H2009-*TBK1* shRNA (3/11). Tumour determination was made at 3 weeks except for NCI-H2009, which were measured at 5 weeks.

TUNEL assay. NCI-H23 cells and NCI-H1437 cells were infected in 96-well plates with shRNAs specific for GFP, *TBK1* and *KRAS*, fixed 5 days after infection using 10% paraformaldehyde, and subjected to TUNEL staining (Roche). Nuclei were co-stained with 4',6-diamidino-2-phenylindole (DAPI), and then imaged and counted using a Zeiss Axiovert 200 immunofluorescence microscope.

Nuclear/cytoplasmic fractionation. Cells were washed twice in ice-cold PBS and incubated on ice for 10 min after treatment with hypotonic cytoplasmic lysis buffer (20 mM HEPES, pH 7.6, 10 mM NaCl, 1.5 mM $MgCl_2$, 0.2 mM EDTA, 1 mM dithiothreitol (DTT), 0.1% NP40 and 20% glycerol) plus proteinase inhibitors. Nuclei were pelleted at 400*g* at 4 °C for 4 min. Supernatants were collected, and the nuclear pellet was washed twice using cytoplasmic lysis buffer. Nuclear lysis buffer (same as cytoplasmic lysis buffer except 500 mM NaCl) was added to the pellet, and samples were incubated for 30 min on ice. After centrifugation at 16,000*g* at 4 °C for 15 min, the supernatant was collected as the nuclear fraction.

Immunoprecipitation. Cells were washed twice with PBS, treated with lysis buffer (50 mM Tris, pH 7.4, 150 mM NaCl, 0.5% NP-40 and 2 mM EDTA) and rotated at 4 °C for 60 min. After centrifugation at 16,000*g*, lysates were quantified. Anti-c-Rel antibody (5 μl) or buffer alone was added to lysate (750 μg) in 500 μl of lysis buffer, and tubes were rotated overnight at 4 °C. Fifty microlitres of 50% protein-G-sepharose beads were added, and samples were incubated for 2 h at 4 °C. After centrifugation at 800*g* for 3 min at 4 °C, beads were washed three times in lysis buffer. Elution was performed using 2× sample buffer, and samples were divided in half and loaded onto parallel gels, along with beads only control and 1/10 input.

Real-time quantitative RT–PCR. Relative mRNA expression was determined using real-time quantitative PCR and normalized to *GAPDH* expression as an internal amplification control. Total RNA was isolated using Trizol reagent (Gibco), and 1 μg of total RNA was reverse transcribed using SuperScript First-Strand Synthesis System (Invitrogen), followed by amplification using SYBR Green PCR Master Mix (Applied Biosystems).

29. Zhang, J. Powerful goodness-of-fit tests based on the likelihood ratio. *J. R. Stat. Soc. Series B Stat. Methodol.* **64**, 281–294 (2002).
30. Sos, M. L. *et al.* Predicting drug susceptibility of non-small cell lung cancers based on genetic lesions. *J. Clin. Invest.* **119**, 1727–1740 (2009).
31. Bhattacharjee, A. *et al.* Classification of human lung carcinomas by mRNA expression profiling reveals distinct adenocarcinoma subclasses. *Proc. Natl Acad. Sci. USA* **98**, 13790–13795 (2001).